12-24-2012

Real time x-ray studies during nanostructure formation on silicon via low energy ion beam irradiation using ultrathin iron films

Osman El-Atwani
Birck Nanotechnology Center, Purdue University, oelatwan@purdue.edu

Anastassiya Suslova
Purdue University, asuslova@purdue.edu

Alexander DeMasi
Purdue University

Sean Gonderman
Purdue University, sean14@purdue.edu

Justin Fowler
Purdue University

See next page for additional authors

Follow this and additional works at: http://docs.lib.purdue.edu/nanopub

Part of the Nanoscience and Nanotechnology Commons

Authors

Osman El-Atwani, Anastassiya Suslova, Alexander DeMasi, Sean Gonderman, Justin Fowler, Mohamad El-Atwani, Karl Ludwig, and Jean Paul Allain

Real time x-ray studies during nanostructure formation on silicon via low energy ion beam irradiation using ultrathin iron films

Osman El-Atwani, Anastassiya Suslova, Alexander DeMasi, Sean Gonderman, Justin Fowler et al.

Additional information on Appl. Phys. Lett.

Real time x-ray studies during nanostructure formation on silicon via low energy ion beam irradiation using ultrathin iron films

Osman El-Atwani,[1,2] Anastassiya Suslova,[3] Alexander DeMasi,[4] Sean Gonderman,[3] Justin Fowler,[3] Mohamad El-Atwani,[3] Karl Ludwig,[4] and Jean Paul Allain[1,2,3]

[1]*School of Materials Engineering, Purdue University, West Lafayette, Indiana 47907, USA*
[2]*Birck Nanotechnology Center, Purdue University, West Lafayette, Indiana 47907, USA*
[3]*School of Nuclear Engineering, Purdue University, West Lafayette, Indiana, 47907, USA*
[4]*Physics Department, Boston University, Boston, Massachusetts 02215, USA*

Real time grazing incidence small angle x-ray scattering and x-ray fluorescence (XRF) are used to elucidate nanodot formation on silicon surfaces during low energy ion beam irradiation of ultrathin iron-coated silicon substrates. Four surface modification stages were identified: (1) surface roughening due to film erosion, (2) surface smoothing and silicon-iron mixing, (3) structure formation, and (4) structure smoothing. The results conclude that 2.5×10^{15} iron atoms in a 50 nm depth triggers surface nanopatterning with a correlated nanodots distance of 25 nm. Moreover, there is a wide window in time where the surface can have correlated nanostructures even after the removal of all the iron atoms from the sample as confirmed by XRF and *ex-situ* x-ray photoelectron spectroscopy (XPS). In addition, *in-situ* XPS results indicated silicide formation, which plays a role in the structure formation mechanism. © *2012 American Institute of Physics.* [http://dx.doi.org/10.1063/1.4773202]

While ion bombardment of compound semiconductors can lead to nanostructure formation of several sizes and shapes,[1–4] structuring of single component semiconductors, in particular silicon, at normal incidence can only occur if a certain level of impurities[5] is deposited on the silicon surface during the irradiation process. Irradiation of silicon surfaces at zero-degree incidence without impurity seeding was shown to smooth silicon surfaces[6] and flatten previously patterned ones.[7] A recent model by Bradley and Shipman[8,9] suggested the importance of immobile impurities on the planar surface instability and the subsequent structure formation on silicon surfaces under normal incidence ion beam irradiation. According to the theory, in the absence of impurity seeding, the ion bombardment momentum transfer to the surface atoms induces surface flow that dominates the curvature-dependent[10] sputter yield, and the surface will smooth. In the presence of impurities, however, the curvature-dependent sputter yield of the impurity-perturbed surface (where impurity atoms sputter more from the valleys) dominates the surface smoothing behavior of the silicon atoms if the impurity flux exceeds a threshold value.

Nanostructuring of silicon surfaces with impurity seeding was mainly studied experimentally by Ozaydin *et al.*[11–13] and Garcia *et al.*[14] These studies conjectured several mechanisms on how impurity seeding can induce nanostructure formation on silicon surfaces at normal incidence irradiation. The conjectured mechanisms included silicide formation, stress generation due to ion bombardment, and variation in the collision cascade. In their cases, however, impurity seeding was performed accidentally (from the ion gun or sample holder clips), and these same impurities remained permanently on the silicon surface. Permanent impurity seeding will render the silicon surfaces unfeasible for future device applications.[15,16] Therefore, it is important to demonstrate if these nanostructures can be formed without permanent impurity seeding. El-Atwani

et al.[17] have shown that structuring (formation of silicon nanodots) of silicon surfaces at normal incidence can occur without the need for permanent impurity seeding by irradiating silicon surfaces coated with a thin film of gold. These results demonstrated that gold-silicon mixing and gold silicide formation occur during irradiation. At the end of the experiment, all the gold atoms were sputtered away from the sample but silicon nanodots remained. The grid of the ion source used for that study was made of graphite, and the sample was raised over the sample holder to mitigate any source of accidental impurity deposition. Moreover, the experiment was performed with *in-situ* x-ray photoelectron spectroscopy (XPS) and low energy ion scattering spectroscopy (LEISS) on the irradiated sample for all fluences, which actively measured any sign of impurities. El-Atwani *et al.*[17] conjectured that silicide formation and the preferential erosion of the non-silicide regions are the key mechanism for the observed nanodots formation. Recently, Macko *et al.*,[18] showed Fe silicide formation close to the elevations of the nanopatterns generated during krypton irradiation of silicon surfaces with Fe co-deposition. Macko *et al.* demonstrated that chemical composition changes due to silicide formation, and the corresponding sputter yield difference between the silicide and the non-silicide regions intensifies the surface height fluctuations due to ion bombardment. Zhang *et al.*[19] also observed higher silicide concentrations in the nanopatterns region during xenon irradiation of silicon substrates with continuous Fe deposition.

In this paper, we extend the work at Purdue University with synchrotron-based real time grazing incidence small angle x-ray scattering (GISAXS) and x-ray fluorescence (XRF). These measurements are performed during argon low-energy ion beam irradiation of thin film (10 nm) iron-coated silicon samples at normal incidence. This real time work elucidates how silicon nanostructures evolve after mixing of metal atoms from the thin film with silicon. The structures

101, 263104-1

remain for higher fluences after removing all the metal atoms from the sample; only with further bombardment does the surface begin to smooth again.

Silicon (100) samples were coated with 10 nm thin films of iron using electron beam deposition in Birck Nanotechnolgy Center (BNC) at Purdue University. The irradiation was performed using a grid broad-beam source (Tectra Gen II) at normal incidence using 200 eV argon irradiation. The ion flux was approximately $1.5\text{-}2 \times 10^{14}\,\mathrm{cm}^{-2}\,\mathrm{s}^{-1}$, and the pressure during irradiation was 8×10^{-4} torr. Irradiation of the samples and the real time GISAXS and XRF experiments were performed on beamline X21 of the National Synchrotron Light Source (NSLS) at Brookhaven National Laboratory (BNL). High-resolution scanning electron microscopy (HRSEM) characterization followed after the removal of the samples from the irradiation chamber. In addition, XPS was performed on the samples to eliminate any doubts about absence of impurities on the samples after irradiation. In another experiment, *in-situ* XPS during the irradiation of 10 nm Fe-coated silicon substrate was also performed to determine the fluence at which mixing starts, and to study the surface chemistry of the system.

Figure 1 shows the real time GISAXS data, plotted as a function of the scattered photon wavenumber ($q_{||}$), during the irradiation process. As demonstrated in the figure, the evolution of nanoscale structures had four stages. In Figure 1(a), sputtering of the iron film and the initiation of iron-silicon

mixing is demonstrated. Development of shoulders at low $q_{||}$ values occurred before and after iron-silicon mixing and up to 560 s of irradiation time. The shoulders indicate kinetic roughening of the sample initiated by the erosion of the iron film, which then started to decay followed by surface smoothing after 1580 s of irradiation time (Figure 1(b)). Just after the smoothing process, silicon nanostructures began to evolve (third stage). The nanostructure formation occurred approximately between 2040 and 3570 s. The evolution of correlated nanostructures is marked by the development of correlation peaks on each side of the central peak in the GISAXS spectra (Figure 1(c)). It should be noted here that the central peak in the GISAXS spectra corresponds to the tail of the specular beam, and the correlation peaks on each side of the central peak correspond to correlated nanoscale structure formation on the samples. The dominant wavelength on the surface, λ, can be approximated as $2\pi/q_{max}$.[20] During the nanostructure formation process, the correlation peak intensity increased with nearly the same $q_{||}$ values indicating that the nanostructures did not coarsen during this time. The highest intensity of the correlated GISAXS peaks was at a value of $q_{||} = 0.25\,\mathrm{nm}^{-1}$, which corresponds to a real space distance of 25 nm between the correlated nanostructures in close agreement with the GISAXS studies performed by Ozaydin *et al.*[11,13] with simultaneous molybdenum deposition. However, coarsening of the nanostructures, as observed in the impurity codeposition studies,[11,21] was not observed. We attribute this observation to
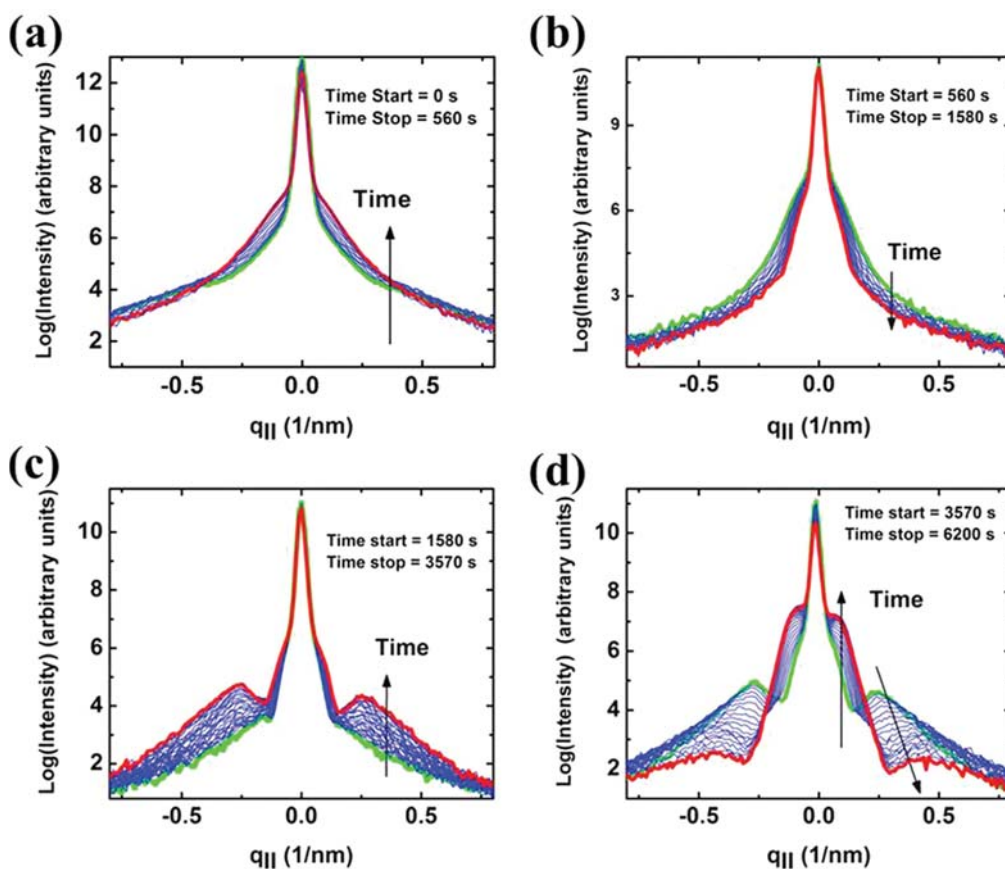
FIG. 1. GISAXS scans of the iron-coated silicon sample irradiated at 200 eV between the irradiation times of (a) 0–920 s, (b) 900–1580 s, (c) 1580–3570 s, and (d) 3570–6200 s. The low $q_{||}$ values peaks (shoulders to the incident peak) indicate long-range correlated structures on the sample. Appearance and disappearance of the low $q_{||}$ value peaks indicate roughening and smoothing of the sample, respectively. The high $q_{||}$ value peaks in ((c) and (d)) and the low $q_{||}$ value peaks in (d) indicate the formation of correlated structures (nanodots).

the difference in the method in which the metal is introduced. In our case, the metal impurities are coming from the film, forming immobilized silicide phases. The surface is then formed of two regions: silicide and non-silicide regions. In the impurity codeposition studies, there is a continuous flux of impurities reaching the surface randomly, and new silicide regions are formed during the growth of the nanostructures.

In the beginning of stage four, after 4000 s of irradiation, all the iron in the sample was removed, as can be seen from Figure 1. The GISAXS correlation peaks (Figure 1(d)) began to decay, while broadening, and moved to higher $q_{||}$ values. At the same time, peaks appeared at low $q_{||}$ values, suggesting two different structural correlations. At nearly 2630 s after the beginning of the smoothing process (6200 s total irradiation time), the GISAXS high $q_{||}$ correlation peaks were still apparent and positioned at a $q_{||}$ value of 0.45 nm^{-1}, which corresponds to a distance of 14 nm between the correlated structures, and evolving low $q_{||}$ value peaks were positioned at 0.1 nm^{-1}, which corresponds to a distance of 62 nm. Just afterward, the correlation peaks started to decay (3570 s of irradiation time), and the high $q_{||}$ (0.45 nm^{-1}) correlation peaks were a little below their maximum intensity (Figure 1(d)). The factors that drive the change in peak position are not exactly known. However, we conjecture that the removal of the immobile silicide regions strengthened the ion-enhanced viscous flow[22] and caused the change in the distance correlation between the dots.

Figure 2 shows the scanning electron microscopy image of the sample after the 6500-s irradiation time (end of stage 4). Dots of less than 8 nm diameter were observed with HR-SEM. The distance between the dots was not uniform. Some dots are very close to each other (separated by less than 20 nm) and others are at a distance of around 60 nm; in agreement with the GISAXS results.

For impurity analysis during the irradiation process, real time XRF was performed on the sample in conjunction with the GISAXS experiment. Figure 3 shows the data output of the real time XRF (Fe-Kα fluorescence) performed on the sample during the ion irradiation process as compared to the time evolution of the GISAXS intensity of the high $q_{||}$ peak. The XRF data were normalized with respect to the elastic scattered peak to adjust for any beam instability. The elastic
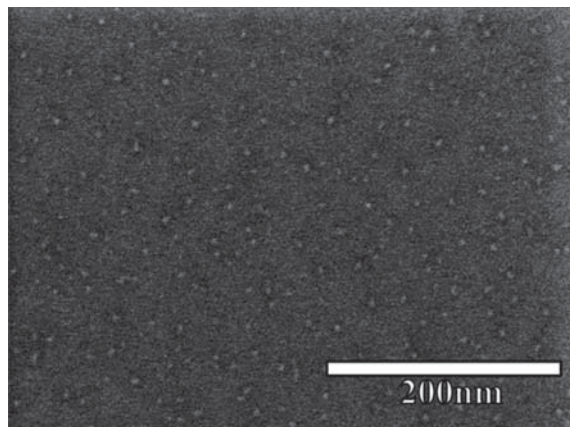
scattered peak is expected to show very small change due to structure evolution (height of the nanodots is in the range of few nms). It should also be noted that the GISAXS intensity is proportional to the Fourier transform of the height-height correlation function, thus it is very sensitive to surface correlations.[5,11] The four stages of the nanodots evolution are marked in the figure. During the first stage, the correlation peak intensity of the correlated peak increased due to the erosion of the film and possible island formation. During this stage, the iron intensity decreases until the 200 eV argon ions are able to penetrate the film and induce mixing with the silicon surface. This occurs after 560 s of irradiation time. The fluence at which mixing starts was also modeled using DYNAMIX (DYNamic transport of multi-atom materials MIXing) code.[23] DYNAMIX is a binary collision approximation (BCA) Monte Carlo code. According to DYNAMIX, mixing between Fe and Silicon should start at 1×10^{17} cm^{-2}. During the second stage, the correlation peak intensity dropped back indicating complete mixing and the start of nanoscale structure formation. At this stage, around 95% reduction of iron concentration is measured (5.2×10^{16} Fe atoms removed and 2.5×10^{15} Fe atoms remaining) by *in-situ* XRF. After that, the evolution of the high $q_{||}$ value nanostructures occurred before iron was completely removed. This is marked by an increase in the GISAXS intensity (third stage), and the highest intensity was observed when all the iron was removed (4000 s). The drop in intensity after that indicated the smoothing behavior of the sample after all the iron was sputtered from the sample (fourth stage). From the GISAXS
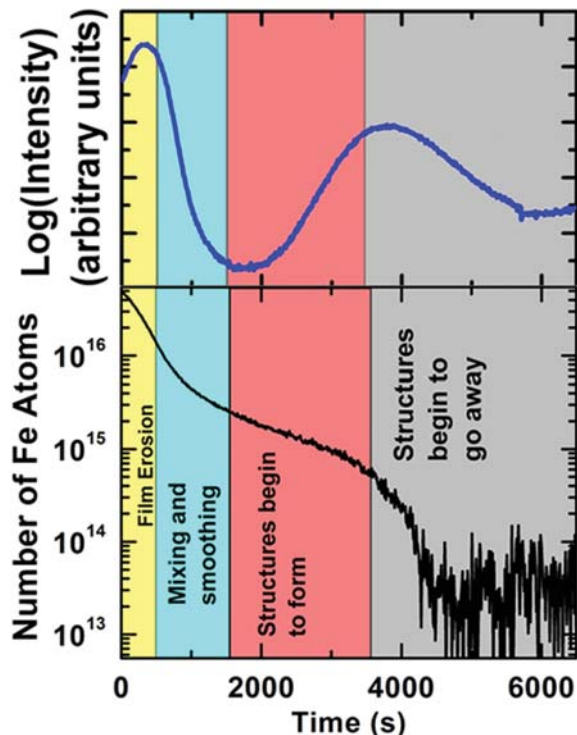
FIG. 3. Comparison of the time evolution of the GISAXS intensity of the high $q_{||}$ value peak and Fe intensity (log-scale) of the real time XRF spectra (Fe-Kα) output of the iron-coated silicon sample irradiated with argon ions at normal incidence and 200 eV. The flux was about 2×10^{14} cm^{-2} s^{-1}, and the irradiation was performed for 6600 s. Evolution of nanodots occurs through four stages as indicated.

FIG. 2. Scanning electron microscopy (SEM) image of the nanostructures formed at the end of the 6600-s irradiation of the iron-coated silicon sample.
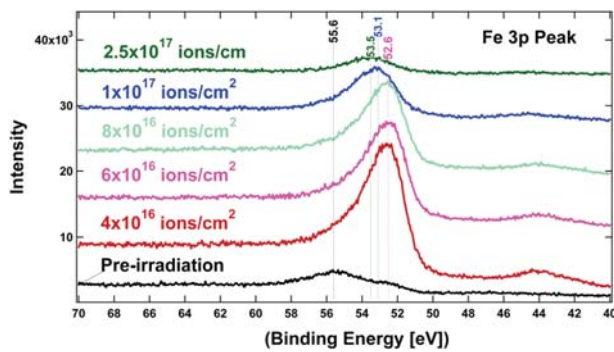
FIG. 4. *In-situ* XPS results (Fe 3p peak), plotted as a function of fluence, of 10 nm Fe-coated silicon substrate irradiated with 200 eV argon.

and XRF results, it is noticeable that there is a wide window in time (Figure 3(d)) where the irradiated sample had correlated nanostructures after the removal of iron. Post-irradiation XPS was performed on the sample to examine the sample purity. The wide scan XPS showed no sign of impurities; the only elements observed were silicon, oxygen, and carbon, confirming the formation of the nanostructures with no permanent metal-impurity seeding. To elucidate the formation mechanism and to determine the exact time interval at which mixing occurs, *in-situ* XPS results during the irradiation of 10 nm Fe-coated silicon substrate are plotted in Figure 4. Before irradiation, iron is in oxide form and Fe 3 p peak is at 55.6 eV. At 4×10^{16} cm^{-2}, the oxide has vanished and Fe is in a pure form (Fe 3 p peak is at 52.6 eV). At 1×10^{17} cm^{-2} and 2.5×10^{17} cm^{-2}, however, the Fe 3 p peak shifts to 53.1 eV and 53.5 eV, respectively, indicating silicon-Fe mixing (at 1×10^{17} cm^{-2}) and the formation of α-FeSi$_2$ and β-FeSi$_2$,[24,25] respectively. The mixing-starting fluence $(1 \times 10.^{17}$ cm$^{-2})$ is in complete agreement with DYNAMIX results mentioned above. Silicide formation, after mixing, and its presence till the removal of Fe atoms, indicates the importance that silicides and phase separation play in the formation mechanism. We conjecture that the structure formation in the presence of iron impurities, which occurred in this stage, was due to possible silicide formation and the preferential erosion of the silicide regions (sputter less)[18] and the non-silicide region (sputter more) in agreement with Macko *et al.* observations. Moreover, silicide formation close to the elevations (tips) should weaken any downward surface flow from the tips to the valleys, which will cause a surface destabilizing effect.

In conclusion, we demonstrated nanostructure formation on silicon samples via ion beam irradiation at normal incidence without permanent impurity seeding for Fe ultra-thin films on Si. *In-situ* and real-time diagnosis of coated Si surfaces indicates four possible stages for effective surface nanostructuring by ion-beam sputtering. The first stage is kinetic roughening of the thin film followed by rapid removal of this film and associated smoothing after silicon-iron mixing. The second stage is a complex balance between ion-induced mixing, silicide formation, and surface smoothing. Once a low level of iron is reached, spontaneous formation of surface nanostructures is observed in the third stage. The final stage is complete removal of Fe atoms and smoothing of the surface Si nanostructures. Removal of the Fe atoms, however, occur before complete smoothing of the surface, and the nanostructures remain for a long time after the removal of all Fe atoms, as indicated by real time XRF and *ex-situ* XPS. Future work will focus on the comparison between silicon substrates coated with different metal films.

[1]S. Facsko, T. Dekorsy, C. Koerdt, C. Trappe, H. Kurz, A. Vogt, and H. L. Hartnagel, Science **285**, 1551 (1999).
[2]A. Hanisch, A. Biermanns, J. Grenzer, S. Facsko, and U. Pietsch, J. Phys. D: Appl. Phys. **43**, 112001 (2010).
[3]O. El-Atwani, J. P. Allain, A. Cimaroli, A. Suslova, and S. Ortoleva, J. Appl. Phys. **110**, 074301 (2011).
[4]S. Le Roy, E. Søndergard, I. S. Nerbø, M. Kildemo, and M. Plapp, Phys. Rev. B **81**, 161401(R) (2010).
[5]G. Ozaydin, K. F. Ludwig, Jr., H. Zhou, L. Zhou, and R. L. Headrick, J. Appl. Phys. **103**, 033512 (2008).
[6]J. Zhou, S. Facsko, M. Lu, and W. Moller, J. Appl. Phys. **109**, 104315 (2011).
[7]G. Ozaydin-Ince and K. F. Ludwig, Jr., J. Phys.: Condens. Matter **21**, 224008 (2009).
[8]R. M. Bradley, Phys. Rev. B **83**, 195410 (2011).
[9]R. M. Bradley and P. D. Shipman, Appl. Surf. Sci. **258**, 4161 (2012).
[10]R. M. Bradley and J. M. Harper, J. Vac. Sci. Technol. A **6**, 2390 (1988).
[11]G. Ozaydin, K. F. Ludwig, Jr., H. Zhou, and R. L. Headrick, J. Vac. Sci. Technol. B **26**, 551 (2008).
[12]G. Ozaydin, A. Ozcan, Y. Wang, K. F. Ludwig, Jr., H. Zhou, and R. Headrick, Nucl. Instrum. Methods Phys. Res. B **264**, 47 (2007).
[13]G. Ozaydin, A. Ozcan, Y. Wang, K. F. Ludwig, Jr., H. Zhou, R. Headrick, and P. Siddons, Appl. Phys. Lett. **87**, 163104 (2005).
[14]J. A. Sanchez-Garcia, L. Vazquez, R. Gago, A. Redondo-Cubero, J. M. Albella, and Z. Czigany, Nanotechnology **19**, 355306 (2008).
[15]R. Takizawa, T. Nakanishi, and A. Ohsawa, J. Appl. Phys. **62**, 4933 (1987).
[16]A. Y. Usenko, US Patent 6, 368, 938 (2002).
[17]O. El-Atwani, S. Ortoleva, A. Cimaroli, and J. P. Allain, Nanoscale Res. Lett. **6**, 403 (2011).
[18]S. Macko, F. Frost, M. Engler, D. Hirsch, T. Hoche, J. Grenzer, and T. Michely, New J. Phys. **13**, 073017 (2011).
[19]K. Zhang, M. Brotzmann, and H. Hofsass, New J. Phys. **13**, 013033 (2011).
[20]G. Renaud, R. Lazzari, and F. Leroy, Surf. Sci. Rep. **64**, 255 (2009).
[21]H. Hofsass and K. Zhang, Appl. Phys. A **92**, 517 (2008).
[22]C. C. Umbach, R. L. Headrick, and K. C. Change, Phys. Rev. Lett. **87**, 246104 (2001).
[23]G. Hou, M.S. Thesis, Purdue University, 2010.
[24]B. Egert and G. Panzner, Phys. Rev. B **29**, 2091 (1984).
[25]M. Nikolaeva, M. Sendova-Vasshileva, D. Dimova-Malinovska, D. Karpuzov, J. C. Pivin, and G. Beshkov, Vacuum **69**, 221 (2002).